IOP Conf. Series: Journal of Physics: Conf. Series **878** (2017) 012031 doi:10.1088/1742-6596/878/1/012031

Concluding Remarks: Connecting Relativistic Heavy Ion Collisions and Neutron Star Mergers by the Equation of State of Dense Hadron- and Quark Matter as signalled by Gravitational Waves

Matthias Hanauske[1,2], Jan Steinheimer[2], Luke Bovard[1], Ayon Mukherjee[2], Stefan Schramm[2], Kentaro Takami[1,4], Jens Papenfort[1], Natascha Wechselberger[1], Luciano Rezzolla[1,2] and Horst Stöcker[*,1,2,3]

[1] Institut für Theoretische Physik, Max-von-Laue-Straße 1, 60438 Frankfurt, Germany
[2] Frankfurt Institute for Advanced Studies, Ruth-Moufang-Straße 1, 60438 Frankfurt, Germany
[3] GSI Helmholtzzentrum für Schwerionenforschung GmbH, 64291 Darmstadt, Germany
[4] Kobe City College of Technology, 651-2194 Kobe, Japan

Abstract. The underlying open questions in the fields of general relativistic astrophysics and elementary particle and nuclear physics are strongly connected and their results are interdependent. Although the physical systems are quite different, the 4D-simulation of a merger of a binary system of two neutron stars and the properties of the hot and dense matter created in high energy heavy ion collisions, strongly depend on the equation of state of fundamental elementary matter. Neutron star mergers represent optimal astrophysical laboratories to investigate the QCD phase structure using a spectrogram of the post-merger phase of the emitted gravitational waves. These studies can be supplemented by observations from heavy ion collisions to possibly reach a conclusive picture on the QCD phase structure at high density and temperature. As gravitational waves (GWs) emitted from merging neutron star binaries are on the verge of their first detection, it is important to understand the main characteristics of the underlying merging system in order to predict the expected GW signal. Based on numerical-relativity simulations of merging neutron star binaries, the emitted GW and the interior structure of the generated hypermassive neutron stars (HMNS) have been analyzed in detail. This article will focus on the internal and rotational HMNS properties and their connection with the emitted GW signal. Especially, the appearance of the hadon-quark phase transition in the interior region of the HMNS and its conjunction with the spectral properties of the emitted GW will be addressed and confronted with the simulation results of high energy heavy ion collisions.

1. Introduction

One hundred years after Albert Einstein developed the field equations of general relativity and predicted the existence of gravitational waves, his theory triumphantly corroborates all experimental and observational tests it has been put through to date. Among the $\approx$ 2500 known neutron stars (NSs), there are some which are in binary systems where the companion of the NS is either a normal star, a planet, a white dwarf or again a NS. The most impressive binary neutron star system, so far[1], is the so called *Double Pulsar: PSR J0737-3039A/B*, which has been discovered in 2003 [2]. The two neutron

[1] An even more relativistic binary pulsar system has been discovered recently and the corresponding experimental results will be reported in the near future [1].

stars in this binary system, which are only separated by 800000 km, orbit around each other with an orbital period of 147 minutes and a mean velocity of one million km/h. This system is excellent for testing Einstein's theory of general relativity and alternative theories of gravity in the strong-field regime [3]. Due to the emission of gravitational waves, the distance between the two NSs decreases with time and finally the two objects will merge accompanied by neutrino radiation, a strong gravitational radiation chirp, and short gamma-ray burst.

Gravitational waves have been recently observed from a pair of merging black holes (BHs) by the LIGO detectors [4, 5] and GWs emitted from merging neutron star binaries are on the verge of their first detection. The main difference between GWs originating from a merger of two BHs or NSs is the possibility of an existence of a post-merger phase after the collisions of the two objects, which can be only present in the case of a NS-merger. Depending on a variety of parameters, e.g. the initial mass of the two stars, the product right after the merger could be a prompt collapse to a BH, a metastable HMNS or a stable supramassive NS. The GWs produced by a merger of NSs are by far more interesting as the GWs resulting from a BH-merger, as, in the case of existence of a post-merger phase, the equation of state (EOS) of elementary matter might be deduced by a frequency analysis of the GW [6, 7, 8]. This is insofar interesting, as the EOS until now is mainly understood by high energy heavy ion collisions and only coarse constraints are coming from astrophysical observations, like the current observational constraint on the observed maximum mass in neutron stars, i.e., $2.01 \pm 0.04 M_\odot$ [9]. In this article we will compare the results of numerical simulations of merging NS binaries with simulations of high energy heavy ion collisions. We will discuss how one can create a similar state of hot and dense nuclear matter in two seemingly different 'experimental' setups, namely the mergers of two neutron stars and relativistic heavy ion collisions. By studying the properties of this QCD natter in a single consistent approach we can finally address one of the most relevant challenges of high-energy nuclear theory. This is to determine the properties and phase structure of QCD at large densities and temperature.

2. Numerical general relativity of neutron star mergers

Einstein's theory of general relativity and the resulting general relativistic conservation laws for energy-momentum in connection with the rest mass conservation are the theoretical groundings of neutron star binary mergers:

$$R_{\mu\nu} - \frac{1}{2} g_{\mu\nu} R \;=\; 8\pi\, T_{\mu\nu}\;,\;\; \nabla_\mu T^{\mu\nu} \;=\; 0\;,\;\; \nabla_\mu \left(\rho\, u^\mu\right) \;=\; 0 \tag{1}$$

$T_{\mu\nu}$ describes the energy-momentum tensor, $R_{\mu\nu}$ is the Ricci tensor, which contains first and second derivatives of the space-time metric $g_{\mu\nu}$, ∇_μ is the covariant derivative and u^μ is the four velocity of the star's fluid. The Einstein equation (first equation in Eq. (1)) describes in which way the space-time structure need to bend (left hand side of the equation) if energy-momentum is present (right hand side of the equation). These highly non-linear differential equations describe on the one hand how matter moves in a curved space-time and on the other hand formulates in which way the amounts of energy-momentum curves the space-time structure. In the ideal-fluid energy-momentum tensor $T_{\mu\nu} = (e+p)\, u_\mu u_\nu + p\, g_{\mu\nu}$ enters the energy and pressure densities of the nuclear and elementary particle physics contributions of the underlying neutron star matter and $u^\mu = dx^\mu/d\tau$ describes the four velocity of the star's fluid which is defined as the derivative of the coordinates $x^\mu = (t, x, y, z)$ by the proper time τ.

The interior metric of a single, spherically symmetric and static neutron star can be calculated by assuming the following Ansatz of the metric $g_{\mu\nu}$ (infinitesimal line element ds)

$$ds^2 \;=\; g_{\mu\nu}\, dx^\mu dx^\nu \;=\; -\, e^{2\nu(r)} dt^2 + \left(1 - \frac{2m(r)}{r}\right)^{-1} dr^2 + r^2 d\theta^2 + r^2 \sin^2\theta\, d\phi^2 \quad . \tag{2}$$

By inserting this Ansatz of the metric and the expression for the energy momentum tensor into Eq. (1) one derives the Tollman-Openheimer-Volkov (TOV) equations (see e.g. [10])

$$\frac{dm}{dr} \;=\; 4\pi r^2\, e\;, \quad \frac{d\nu}{dr} \;=\; \frac{m + 4\pi r^3 p}{r\,(2m - r)}\;, \quad \frac{dp}{dr} \;=\; -\,(e+p)\frac{d\nu}{dr} \quad . \tag{3}$$

For a given equation of state (EOS: a function $p(e)$) the TOV equation can be solved numerically by fixing the central pressure p_c and integrating outwards to the star's surface where the pressure is zero. It can be shown (Birkov Theorem, see e.g. [11], page 843f) that the metrical structure outside the neutron star is identical to the Schwarzschild metric of a black hole. It is impressive that Karl Schwarzschild found this analytical solution of the Einstein equation only three month after Einstein's article and it is very unfortunate that he died soon after his remarkable result. The Schwarzschild solution is only valid in a spherically symmetric approximation and even for a single rotating neutron star the metric outside the body cannot be described analytically, as a similar theorem like the Birkov Theorem does not hold for the Kerr solution of a rotating black hole. However, all of the known NSs, including the individual stars of the famous double PSR J0737-3039A/B, can be described in good approximation with the TOV equations and only in the case of a very cramped binary system tidal deformations become important.

In order to solve the evolution of a merging neutron star binary system numerically, Eq. (1) needs to be rewritten, because its structure is not well posed. To reformulate Eq. (1), the so called $(3+1)$-split is used, which starts by slicing the 4-dimensional manifold $\mathcal{M}$ into 3-dimensional space-like hypersurfaces Σ_t. The space-time metric $g_{\mu\nu}$ is then sub-classified into a purely spatial metric γ_{ij}, a lapse function α and a shift vector β_i ($\mu, \nu = 0, 1, 2, 3$ and $i, j = 1, 2, 3$):

$$g_{\mu\nu} \;=\; \begin{pmatrix} -\alpha^2 + \beta_i\beta^i & \beta_i \\ \beta_i & \gamma_{ij} \end{pmatrix} . \tag{4}$$

The lapse function α describes the difference between the coordinate time t and the proper time of a fluid particle τ ($d\tau = \alpha\, dt$). The shift vector β_i measures how the coordinates are shifted on the spatial slice if the fluid particle moves an infinitesimal time step further. In the case of a rotating neutron star, this shift vector formulates one important difference between Newtonian gravity and general relativity - the dragging of local inertial frames in the case of a rotating body. The Lensing-Thirring effect, which has its nature in this property, has been experimentally proved [12] and the gravitomagnetic effect, which corresponds to a general relativistic counterpart of the Lorentz force has been indirectly verified in the binary system PSR 1913+16.

By inserting the metric (4) into the Einstein equation (1) one can restate the equations into a system of first order differential equations, the so called Arnowitt-Deser-Misner (ADM) equations. As the ADM equations are still not 'well posed' (for details see [10]), they need to be further transformed using a conformal traceless formulation. In this article we follow the 'well posed' Baumgarte-Shapiro-Shibata-Nakamura-Oohara-Kojima (BSSNOK) formulation [13, 14] of general relativity. This BSSNOK formulation of general relativity together with the relativistic hydrodynamical equations are finally used as the grounding equations in our computer program [15, 16].

In the following, the results of two simulations will be presented. The EOS used within the first framework is composed of a cold nuclear-physics part and a thermal ideal fluid component (for details see [17, 7]). The cold part have been modelled by a hybrid star matter model (`ALF2-EOS` [18]), where a phase transition to color-flavor-locked quark matter has been implemented. Within this model, the hadronic particles begin to deconfine to quark matter above a certain transition rest-mass density $\rho_{\mathrm{trans}} = 3\,\rho_0$, where $\rho_0 := 2.705 \times 10^{14}$ g/cm^3 is the nuclear-matter rest-mass density. Assuming a moderate surface tension of the quark matter droplets, a phase transition is implemented by using a Gibbs-construction (for details see e.g. [19]). As charge neutrality is only globally conserved within this construction, a mixed-matter phase exists in the rest-mass density range $3\,\rho_0 \leq \rho \leq 7.8\,\rho_0$. The EOS used within the second simulation is the purely hadronic but temperature dependent Lattimer-Swesty EOS (`LS220-EOS` [20]). The initial coordinate separation of the stellar centers has been set to $45\,\mathrm{km}$ for both models. For each EOS, two equal-mass binaries have been considered, where the (gravitational) mass of each star at infinite separation has the value of $M_{\mathrm{In}} = 1.35 M_\odot$ for the `ALF2-M135` run and $1.32 M_\odot$ for the `LS220-M132` simulation.

The results of 4-dimensional numerical simulations of merging neutron star binaries in full general relativity (see Fig. 1) show that the emitted GWs of the merger and post-merger phase are strongly

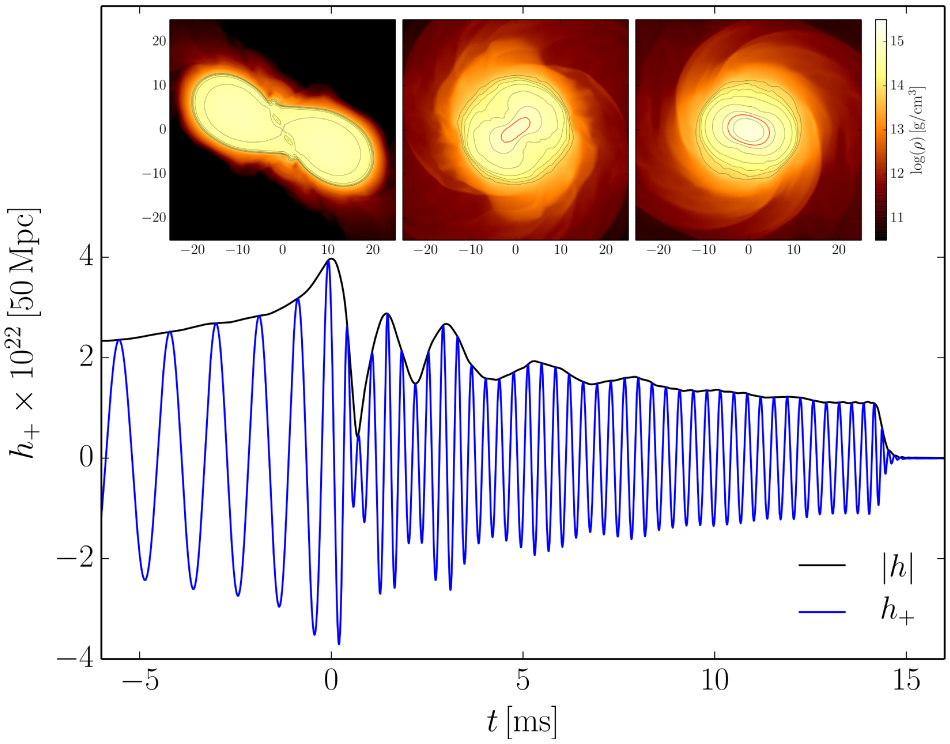

Figure 1. Rest mass density profiles on the equatorial plane and gravitational wave amplitude $|h|$ and h_+ at a distance of 50 Mpc for the ALF2−EOS with $M_{\rm In} = 1.35 M_\odot$.

determined by the high density region of the EOS. The underlying general-relativistic hydrodynamical evolution of the produced HMNS depends on the hadronic and quark matter properties, which also enters in heavy ion collisions (see Sec. 3). Fig. 1 depicts the GW-amplitude of of the ALF2−M135 run. The absolute maximum of $|h|$ marks the time of the merger (i.e., $t = 0$ ms) and the last peak of h_+ corresponds to the time where the HMNS collapses to a black hole (i.e., $t = 14.16$ ms). The upper part of Fig.1 shows the logarithm of the rest mass density profiles for three different time snap-shots ($t = -0.17, 4.05, 13.16$ ms), whereat the boundary of the hadron-quark phase transition (HQPT) is marked with a red curve. For the used ALF2−EOS with $M_{\rm In} = 1.35 M_\odot$, the maximum density reached within the inspiral phase is below the onset of the HQPT, but soon after the merger the density reaches values above $\rho_{\rm trans}$, forming a mixed phase inner region of deconfined quark matter. The detection of GWs from merging neutron star binaries can be used to determine the high density regime of the EOS. The power spectral density profile of the post-merger emission is characterized by distinct frequency peaks and with the knowledge of the total mass the system, the GW signal can set tight constraints on the EOS (see [6, 7, 8] for a definition and discussion of the various frequencies of the post-merger signal).

While the produced HMNS of the ALF2−M135 run collapses to a BH, no gravitational collapse happens for the LS220−M132 run within our simulation time domain. Fig. 2 shows a comparison between the two simulations in respect to the evolution of the minimum value of the lapse function $\alpha_{\rm min}$ and the maximum magnitude of the rest mass density $\rho_{\rm max}$. The collapse to the final BH in the ALF2−M135 case, can be easily seen as a sudden increase in $\rho_{\rm max}$ (sudden decrease in $\alpha_{\rm min}$). In contrast, the LS220−M132 run does not collapse to a BH but evolves to a quasi-stable HMNS. Fig. 3 shows the density and temperature profiles of the HMNS at a post-merger time of $t = 6.34$ ms. Additionally, in Fig. 3, the flowlines tracked by massless tracer particles that are advected in the flow are visualized in

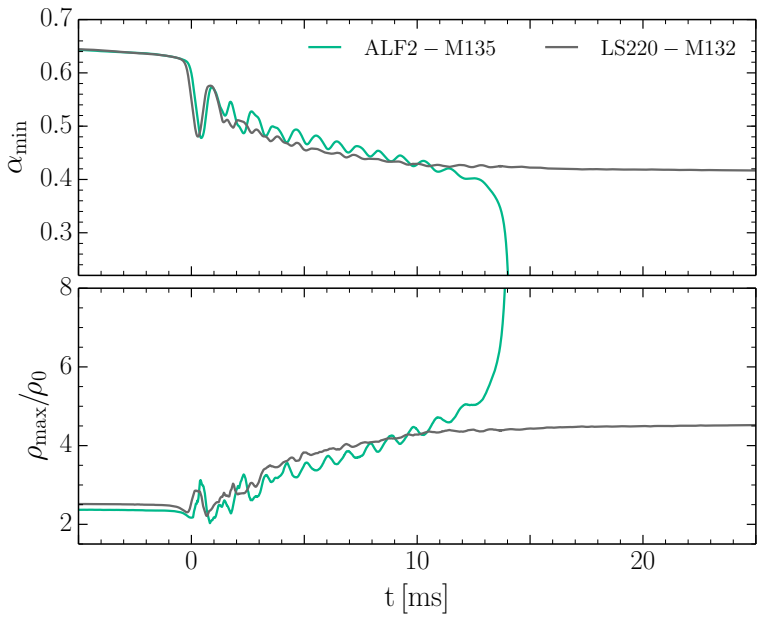

Figure 2. Minimum value of the lapse function $\alpha_{\rm min}$ (upper panel) and maximum of the rest-mass density $\rho_{\rm max}$ in units of the nuclear-matter rest-mass density ρ_0 (lower panel) versus time in milliseconds after the merger for the `ALF2-M135` and `LS220-M132` simulations. Before the merger, the maximum (central) value of the rest-mass density is essentially constant. In the transient post-merger phase strong fluctuations of $\rho_{\rm max}$ and $\alpha_{\rm min}$ occur, while during the "post-transient" phase, $\rho_{\rm max}$ ($\alpha_{\rm min}$) show a quite regular oscillating behaviour with an average increasing (decreasing) value.

the corotating frame of the rest-mass density (for details on the implementation of tracers see [21, 22]). The fluid trajectories indicate that the temperature hot spots also represent vortices around which fluid elements rotate. In order to understand the temperature profile and underlying reason of the curious tracer paths, the angular velocity distribution Ω is visualized in Fig. 4. The temperature and Ω distributions bear a remarkable similarity and the position of the hot spots overlaps closely with the position of the maxima

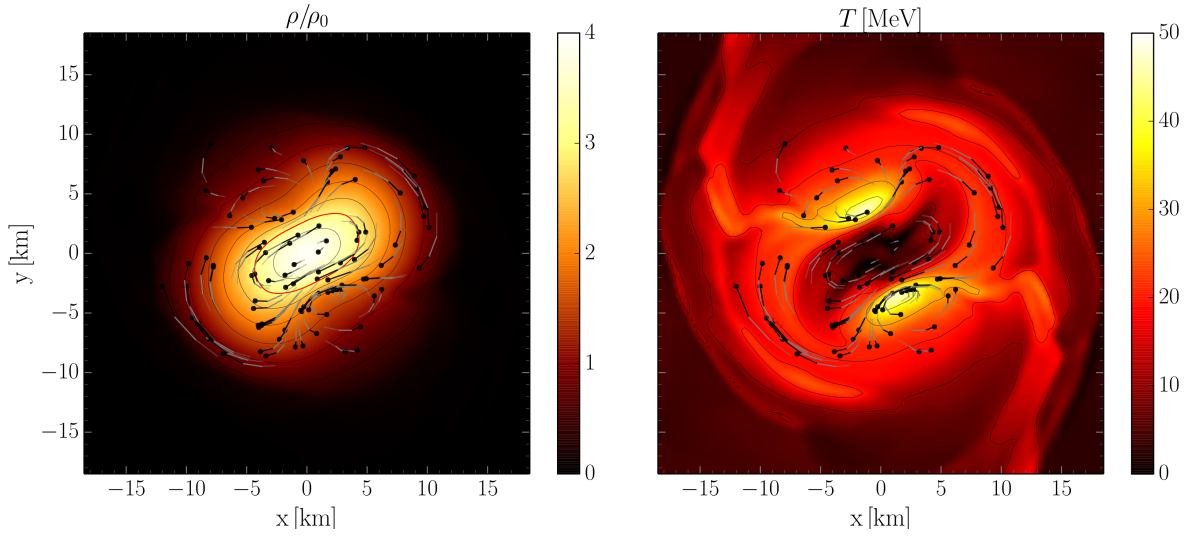

Figure 3. Distributions of the rest-mass density ρ in units of ρ_0 (left panel) and the temperature (right panel) on the equatorial plane at a post-merger time of $t = 6.34$ ms for the `LS220-M132` binary. Also shown are portions of the flowlines of several tracer particles that remain close to the (x, y)-plane and for which we show only the final part of the flowlines. In the left picture, the black isocontours have been drawn at $\rho/\rho_0 = 0.5n$ ($n \in \mathbb{N}$), while the red isocontour indicates $\rho = 3\,\rho_0$. The temperature isocontours (right picture) have been drawn at $T = 10n$ MeV.

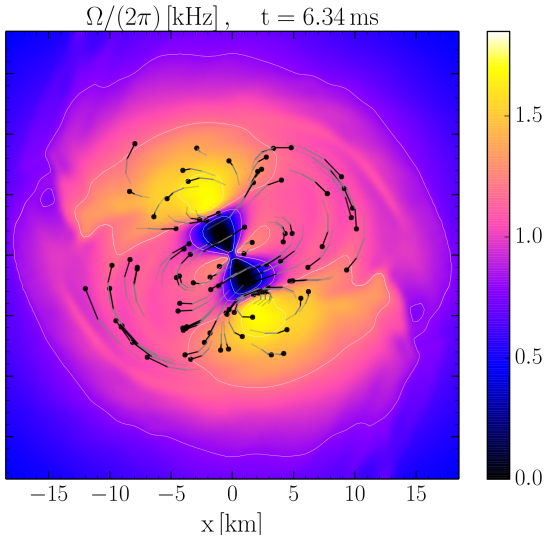

Figure 4. Angular velocity distribution Ω on the equatorial plane at a post-merger time of $t = 6.34$ ms for the `LS220-M132` binary. Ω, which is defined as $\Omega := \frac{d\phi}{dt} = \frac{u^\phi}{u^t} = \alpha\, v^\phi - \beta^\phi$ consists of a lapse-corrected part of the ϕ-component of the three-velocity, minus a frame-dragging term provided by the ϕ-component of the shift vector. The figure shows that the HMNS is a strongly differentially rotating object whereat the two maxima appear at a radial distance of $\simeq 6$ km, while the inner core is rather slowly rotating. The largest gradients in the Ω-profile take place at the positions of the temperature hot spots. The white isocontours have been drawn at $\Omega = [0.4, 0.8, 1.2, 1.6]$ kHz.

in the angular-velocity distribution. Furthermore, the profiles for ρ and Ω show a $m = 2$ deformation, however, they have a phase offset of $\simeq 90$ degrees between them. The physical cause of this phase offset and the underlying reason of the hot spots can be explained rather simply with the Bernoulli's theorem for which areas of low rest-mass density (pressure) are accompanied by regions of large velocity (for details see [23]).

For later times the HMNS reaches a stationary state, the two hot spots disappear and the temperature distribution reaches an axisymmetric pattern. Interestingly, the high-temperature region is not the central one, which is slowly rotating and comparatively colder, but appears at an annular region at about 7-8 km from the center. The figures A1 and A2 in the Appendix A show the rest-mass density ρ and the

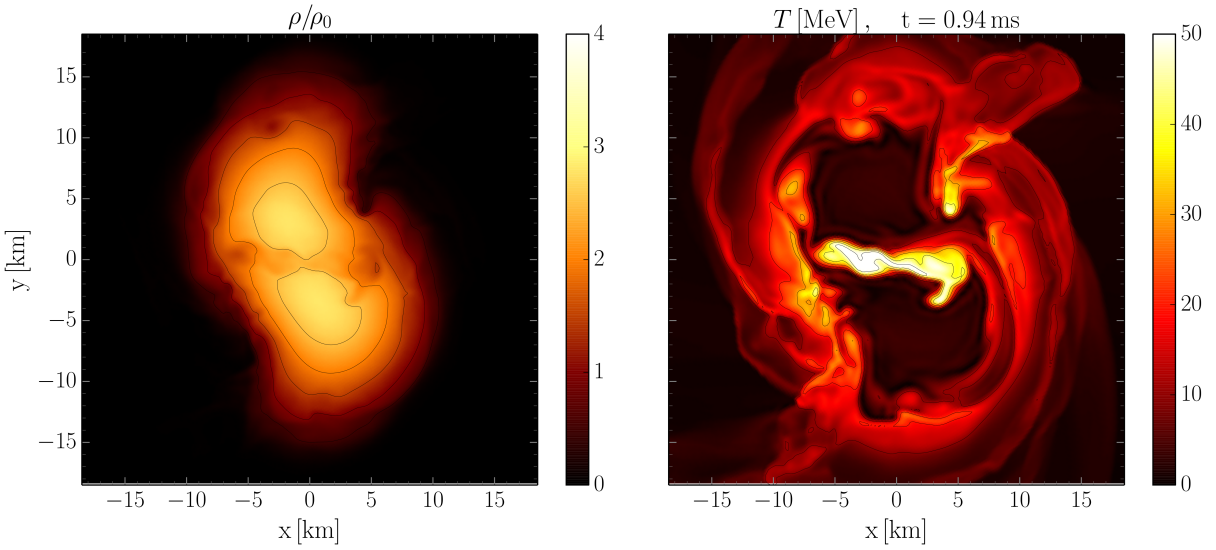

Figure 5. Distributions of the rest-mass density ρ in units of ρ_0 (left panel) and the temperature (right panel) on the equatorial plane at a post-merger time of $t = 0.94$ ms for the `LS220-M135` binary. In the left picture, the black isocontours have been drawn at $\rho/\rho_0 = 0.5n$ ($n \in \mathbb{N}$). The temperature isocontours (right picture) have been drawn at $T = 10n$ MeV.

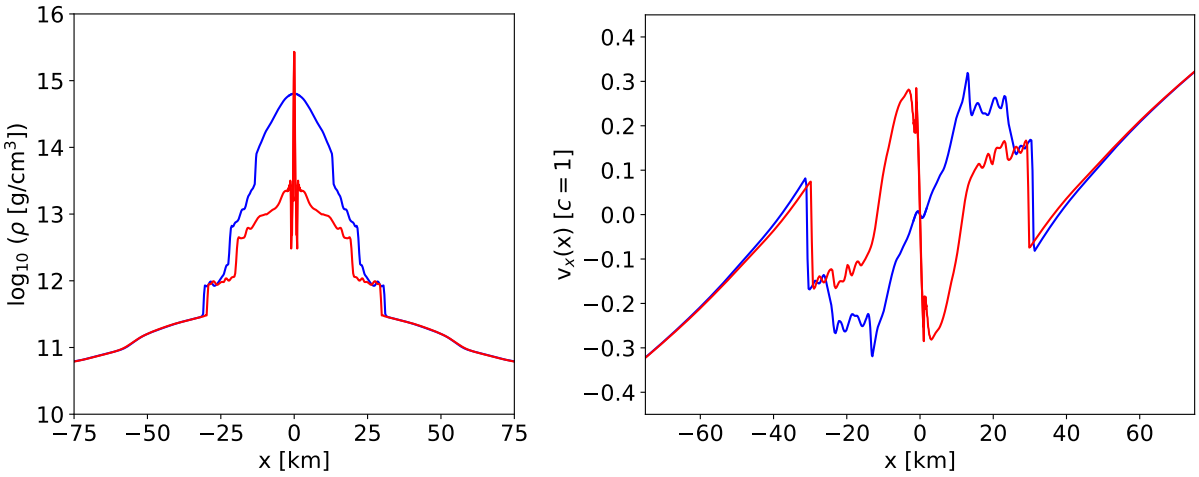

Figure 6. Density (left panel) and velocity (right panel) profiles for head on mergers of NSs. The snapshots are taken at a time $t = 1.4$ ms. We compare collisions where a black hole is formed (red line) and collisions where a NS remnant remains (blue line).

temperature profile at a post-merger time of $t = 11.54$ ms and $t = 23.83$ ms.

However, within the transient post-merger phase ($0 < t < 3$ ms) the temperature hot spots appear in the central area of the inner core of the HMNS and could reach values up to $T \approx 100$ MeV. Fig. 5 shows the density and temperature distributions 0.94 ms after merger. The equatorial density profile (left picture) indicate clearly that the HMNS, at this early phase, has still a double core structure and the high temperature region is located between these density maxima. The underlying simulation of Fig. 5 has been set up with slightly different initial conditions ($M_{\rm In} = 1.35 M_{\odot}$, for details see [23]) but the main characteristics of the described density and temperature structures of the different post merger phases are independent on the EOS or initial mass of the binary, if the merger product does not immediately collapse to a BH due to a to heavy initial mass.

Figure 6 shows the density and velocity profiles of neutron star matter in a head on merger of two NSs. Note the considerable radial acceleration of the matter at the shock fronts of the colliding neutron star matter slabs, which yields in a millisecond time step relative flow velocities above 0.5 c - and densities of several times the central density of the separated NSs. These velocities are close to the velocities and densities achieved in relativistic heavy ion collisions at the GSI and FAiR accelerators, but below those at RHIC and the LHC.

In the following section we will present, for those accelerator energies, the compressions achieved in relativistic nuclear collisions. By using different models for the dynamical description of the compressional phase, with a realistic EOS for hot and dense nuclear matter, we can make a connection from heavy ion collisions to the matter created in NS mergers.

3. The hot and dense QCD equation of state for heavy ion collisions and neutron star mergers

As we have seen, the densities created in the mergers of compact stars can exceed several times the nuclear ground state density. Furthermore we have shown that in the early time of the merger high temperatures $T \leq 100$ MeV are obtained. The properties of matter at such high temperature and density are very different from what we expect from cold nuclear matter. In fact we know that similar densities and temperatures can be created in the relativistic collisions of heavy nuclei at different particle accelerators. In such heavy ion experiments the heavy nuclei are accelerated to relativistic velocities. As they collide, they create a small system (of several fm in size and a lifetime of approximately 20 fm/c) which is expected to have a temperature of $T \geq 80$ MeV and densities several times the nuclear

ground state density. It is therefore very intriguing to study QCD matter at similar temperatures and densities in two rather different 'experimental' setups, in neutron star mergers and heavy ion collisions. By combining the findings from both observations one may be able to deduce information on the properties of the QCD matter at high densities and finally on the phase structure of QCD. The properties of the equation of state of QCD are the link connecting the neutron star mergers and relativistic nuclear collisions. Consequently the goal of such studies has to be to find a description for the EOS that is able to describe neutron star merger and nuclear collision observables and therefore establish the connection.

In the following we will introduce such a model for hot and dense QCD matter and discuss how it is constructed. But first we have to establish common features and differences of the systems created in heavy ion collisions and neutron star mergers. For that we estimated the expected maximal compression reached in nuclear collisions at different colliding beam energies. Since the very early stage of a nuclear collision is a very rapid and violent process, expected to take place out of thermal equilibrium, estimating the maximal compression is no unambiguous task. We compare the energy and net baryon densities reached, as function of the colliding beam energy per nucleon pair $\sqrt{s_{NN}}$ in figures 7. Here we use different methods, which do not depend on the EOS, to estimate these densities.

The dashed lines follow from a simple geometric overlap model where one assumes that the total energy and baryon number of the nuclei, colliding head on, is completely stopped in a volume which is equal to the Lorentz contracted volume of a singe nucleus. The expected densities then can be written as:

$$\rho_{\rm ini} = 2\,\gamma_{\rm c.m.}\,\rho_0 \quad \text{and} \quad \epsilon_{\rm ini} = 2\,m_N\,\rho_0\,\gamma^2_{\rm c.m.} \tag{5}$$

where ρ is the net-baryon density, ϵ is the energy density, $\gamma_{\rm c.m.}$ is the Lorentz gamma of the nuclei in the center of mass (c.m.) frame of the collision and m_N is the nucleon mass. The densities from the geometric overlap model serve as a lower bound of the expected densities since this simple approach does not take into account the additional compression which occurs as the two nuclei penetrate each other.
To get a more realistic estimate for the initial compression we also show results where a microscopic transport model is used to simulate the initial non-equilibrium compression stage (grey band in figures

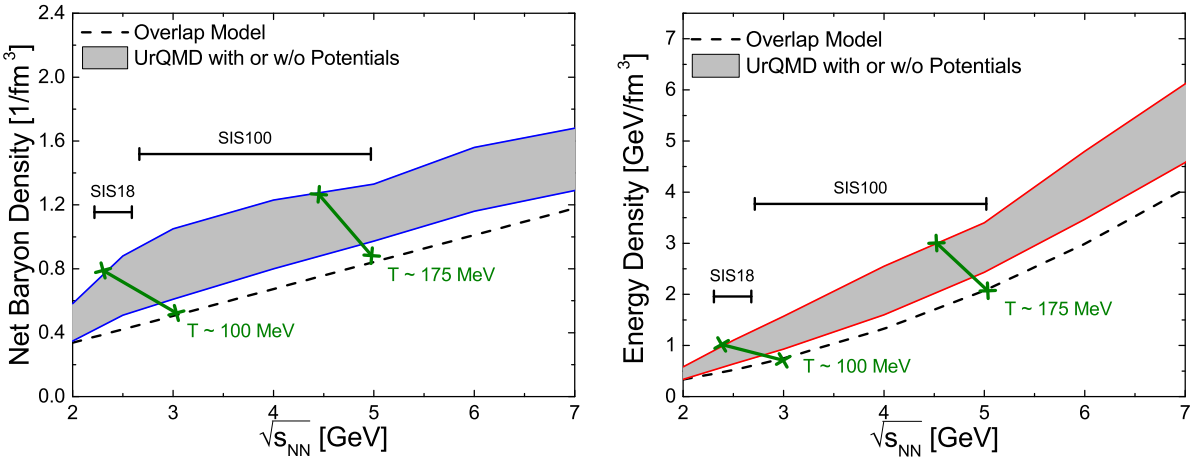

Figure 7. Left: Largest net-baryon densities achieved in central collisions of Au+Au nuclei at different colliding beam energies. Right: Largest energy density achieved in central collisions of Au+Au nuclei at different colliding beam energies. For both figures we compare results from an overlap model (dashed black line) with results where we used the UrQMD model to estimate the initial compression. The green lines with crosses indicate the beam energies where we expect the maximal temperature to exceed 100 or 175 MeV. The temperatures are calculated using the QχP model described in the text.

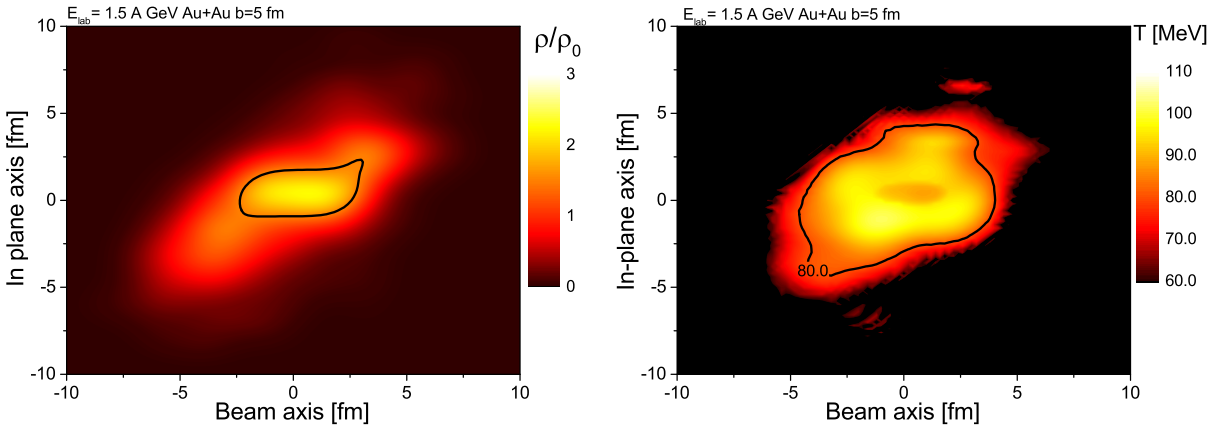

Figure 8. Left: Net baryon density contour in the reaction plane of a non-central (b= 5 fm) nuclear collision of Au+Au nuclei at a beam energy of $E_{\rm lab} = 1.5$ A GeV. The contour where the density exceeds two times nuclear ground state density is highlighted (black dashed line). The densities where calculated using the UrQMD transport model. Right: Same as left but for the temperature. The temperature has been calculated from the density and energy density using the QχP model for the equation of state.

7). The Ultrarelativistic Quantum Molecular Dynamics Model (UrQMD) is used in its cascade mode as well as a setup that includes nuclear interactions via potentials [24, 25]. To obtain a smooth density distribution from the microscopic model we run a large number of events and average densities over this event-ensemble. The so obtained values of the densities are generally larger, by up to a factor of 2, than the values of the overlap model. We find that is we want to study systems that have densities of approximately 4 times the nuclear ground state density $\rho \approx 0.6 fm^3$ we have to study systems created at beam energies of $\sqrt{s_{\rm NN}} \approx 2.5 - 3.0$ GeV. This is the energy region of the current SIS18 accelerator at GSI, as can be seen in figures 7.

As in the case of neutron star mergers the spatial density distribution in nuclear collisions is far from uniform. While in the center of the collision zone very high densities and temperatures can be obtained, we also observe a steep gradient of the densities. To illustrate this we show in figures 8 contour plots of the net-baryon density and the corresponding temperatures for collisions of Au+Au nuclei at a fixed target beam energy of 1.5 A GeV, as expected for the SIS18 accelerator. This snap-shot of the densities as taken at a time $t = 15 fm/c$, a time where one expects the system to be at least partially in local equilibrium. Again we observe that the bulk of the system reaches densities ranging from 1 to 4 time nuclear ground state density and temperatures from 50 to 100 MeV.

It is important to note at this point that in order to extract the temperature of the system at given densities, one requires knowledge on the effective degrees of freedom of the system, encoded in the equation of state. So depending on the EOS the temperatures reached in these relativistic collisions may vary significantly. It is therefore most important to employ an EOS that entails a realistic set of degrees of freedom as well as interactions. In the following we will present a model for such an EOS which can be employed to describe the matter produced in neutron star mergers as well as heavy ion collisions, thus an EOS which is able to link the properties of collision events in drastically different environments.

3.1. The QχP model

The model we employed is the so called Quark-Hadron Chiral Parity Doublet Model (QχP) [26, 27]. In this approach, an explicit mass term for baryons in the Lagrangian is possible, which preserves

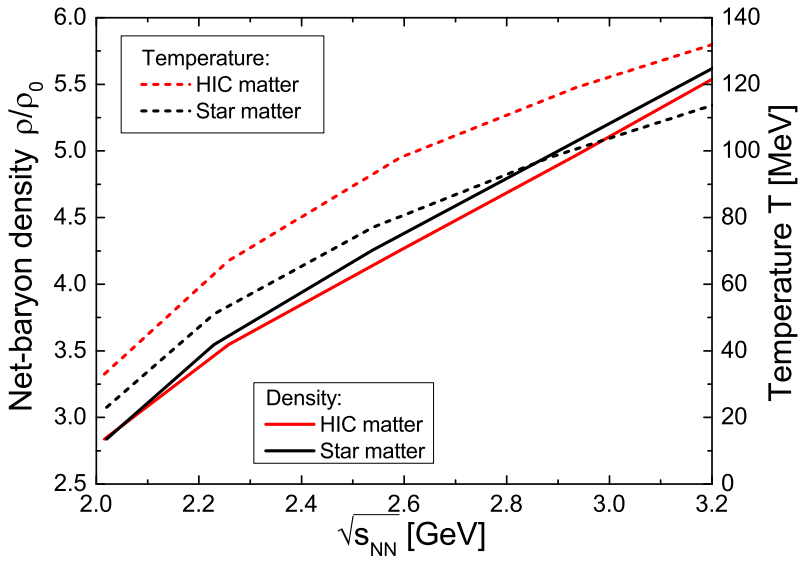

Figure 9. Largest net-baryon density (solid lines) and temperatures (dashed lines) achieved in collisions of heavy ions and compact stars at a given center of mass beam energy $\sqrt{s_{\rm NN}} = 2 \cdot \gamma_{\rm c.m.} \cdot m_N$. To calculate the densities and temperatures we used the Taub adiabat (see text) with the QχP EOS. Due to the different properties of the EOS as function of iso-spin the temperatures in heavy ion collisions are larger and densities slightly smaller, at the same relative velocities.

chiral symmetry. Chiral symmetry is considered one of the most important features of QCD and the restoration of chiral symmetry may be deeply connected with the deconfinement phase transition. The chiral condensate serves as order parameter of the chiral transition and is the only well defined order parameter in QCD thermodynamics.
In the (QχP) model, the signature for chiral symmetry restoration is the degeneracy of the usual baryons and their respective negative-parity partner states. The positive and negative parity states of the SU(3)$_f$ baryons are grouped in doublets $N = (N^+, N^-)$ as discussed in [28, 29].

Taking into account the scalar and vector condensates in mean-field approximation, the resulting Lagrangian $\mathcal{L}_{\mathcal{B}}$ includes [27]

$$\begin{aligned} \mathcal{L}_{\mathcal{B}} &= \sum_i (\bar{B}_{\rm i} i\partial\!\!\!/ B_{\rm i}) + \sum_i \left(\bar{B}_{\rm i} m_{\rm i}^* B_{\rm i}\right) \\ &+ \sum_i \left(\bar{B}_{\rm i} \gamma_\mu (g_{\omega {\rm i}} \omega^\mu + g_{\rho {\rm i}} \rho^\mu + g_{\phi {\rm i}} \phi^\mu) B_{\rm i}\right) \ , \end{aligned} \tag{6}$$

summing over the states of the baryon octet. Furthermore the scalar meson interaction, driving the spontaneous breaking of the chiral symmetry, is expressed in terms of SU(3) invariants $I_2 = (\sigma^2 + \zeta^2)$, $I_4 = -(\sigma^4/2 + \zeta^4)$ and $I_6 = (\sigma^6 + 4\zeta^6)$ as:

$$V = V_0 + \frac{1}{2} k_0 I_2 - k_1 I_2^2 - k_2 I_4 + k_6 I_6 \ , \tag{7}$$

where V_0 is fixed by demanding a vanishing potential in the vacuum. The quark and gluonic degrees of freedom are introduced as done in the PNJL approach [30, 31]. This model uses the Polyakov loop Φ field to describe an effective thermal de-confinement. To suppress hadrons in the deconfined phase we also introduced a simple excluded volume for the hadrons. The various parameters of this model are fixed by demanding a reasonable description of nuclear ground state properties like the saturation density, binding energy and symmetry energy. Furthermore if this model is extended to finite temperature and vanishing chemical potentials it gives a reasonable qualitative description of lattice QCD thermodynamics. A more detailed description of this model, can be found in [26, 27].

This model is highly qualified to study the properties of matter at high densities and intermediate temperatures, as expected in nuclear collisions as well as neutron star mergers. Within the same

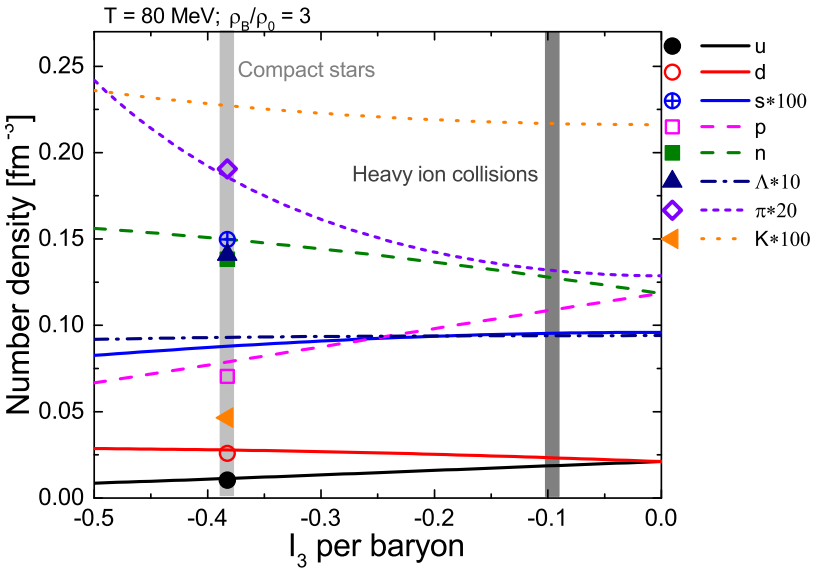

Figure 10. Number densities of different hadronic and free quark species (rescaled for visibility) as function of the iso-spin per baryon at a fixed temperature T=80 MeV and net-baryon density $\rho = 3\rho_0$. The lines correspond to matter with conserved net strangeness, as expected for heavy ion collisions while the symbols represent results where the matter is on β-equilibrium (as expected for neutron star matter).

parameter set we can use this model to calculate the EOS and chemical properties of QCD matter. A straight forward way of connecting the features of the EOS with the maximally achievable compression of a relativistic collision is by employing the so called Rankine-Huguniot-Taub-Adiabat [32]. The Taub adiabiat is essentially a shock wave solution of two colliding infinite slaps of matter. If the EOS, i.e. the connection between pressure, energy density and baryon density is know (as p(ϵ,ρ)), then one can calculate the maximum compression in a collision by solving the following Taub-equation:

$$(\rho_0\, X_0)^2 - (\rho\, X)^2 - (p_0 - p)(X_0 + X) = 0 \tag{8}$$

with $X = (\epsilon + p/\rho^2)$, the generalized volume. For simplicity we assume $p_0 = 0$. One can furthermore connect the center of mass gamma factor $\gamma_{\rm c.m.}$ of the colliding slabs to the densities created:

$$\gamma^2_{\rm c.m.} = \left(\frac{\epsilon\, \rho_0}{\rho\, \epsilon_0}\right)^2 \tag{9}$$

The resulting beam energy dependence of the net-baryon density and temperatures reached is shown in figure 9 for two different scenarios:

(i) The EOS for heavy ion collisions, i.e. with conserved strangeness and no beta-equilibrium
(ii) The EOS for compact stars, i.e. in beta-equilibrium

Again we observe that the densities and temperatures achieved in this consistent approach are similar to those discussed earlier. An important observation is that the density compression in iso-spin symmetric matter and NS matter is very similar the actual temperature is quite different. The reason for this difference are the additional degrees of freedom, i.e. leptons in beta equilibrium and non-conserved strangeness, which decrease the temperature at a given compression. Again this highlights the importance to employ a consistent and realistic temperature dependent EOS for the description of NS matter. Eventually this EOS can also be used in full 3+1D fluid dynamical simulations of heavy ion collisions. As in the NS merger simulations the goal here is to possibly find observables for a (non-equilibrium) first order phase transition in dense QCD matter [33].

To highlight similarities and differences in the chemical composition of the systems created in these collisions we show in figure 10 the number densities of different hadronic species at a fixed temperature and net-baryon density, as function of the iso-spin per baryon of the system. This stresses the different composition of systems created in collisions of Au+Au nuclei (where the iso-spin per baryon is -0.1) and

of neutron star matter. The matter in neutron stars not only has a an iso-spin per baryon of -0.38 but also, according to beta equilibrated strangeness, a significantly different composition of strange particles.

4. Conclusions

In this article we show that the properties of elementary matter at high temperatures ($T \approx 100$ MeV) and densities ($\rho \approx 3\,\rho_0$) can be studied in two different physical scenarios. High energy heavy ion collision experiments try do determine the phase structure of the iso-spin symmetric QCD equation of state, and the knowledge of the iso-spin asymmetric QCD-EOS is needed in a general relativistic computer simulation of binary neutron star mergers. These two different fields of physics, namely elementary particle physics and astrophysics, combine when two neutron stars collide. It is therefore possible to study the properties of dense QCD for systems of different size, time-scales and chemical composition, which will eventually lead to an understanding of the properties of this elementary form of matter.

Acknowledgements

Support comes from "NewCompStar", COST Action MP1304, from the LOEWE-Program in HIC for FAIR, and from the European Union's Horizon 2020 Research and Innovation Program (Grant 671698) (call FETHPC-1-2014, project ExaHyPE). MH gratefully acknowledges support from the Frankfurt Institute for Advanced Studies (FIAS) and the Goethe University Frankfurt, while HS acknowledges the Judah M. Eisenberg laureatus Professur endowment. The simulations were performed on SuperMUC at LRZ-Munich, on LOEWE at CSC-Frankfurt and on Hazelhen at HLRS in Stuttgart.

Appendix A. Evolution of the density and temperature distributions in the late post merger phase

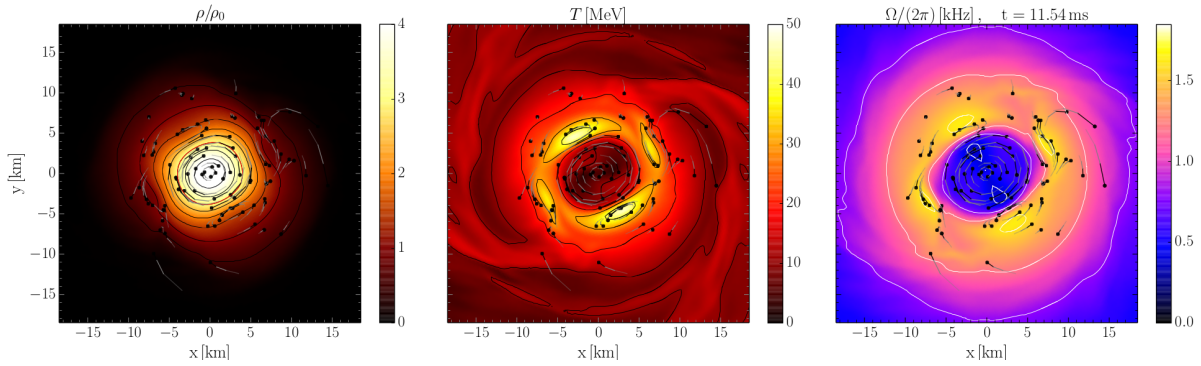

Figure A1. Same as in Figs. 3 and 4 but at a post-merger time of $t = 11.54$ ms.

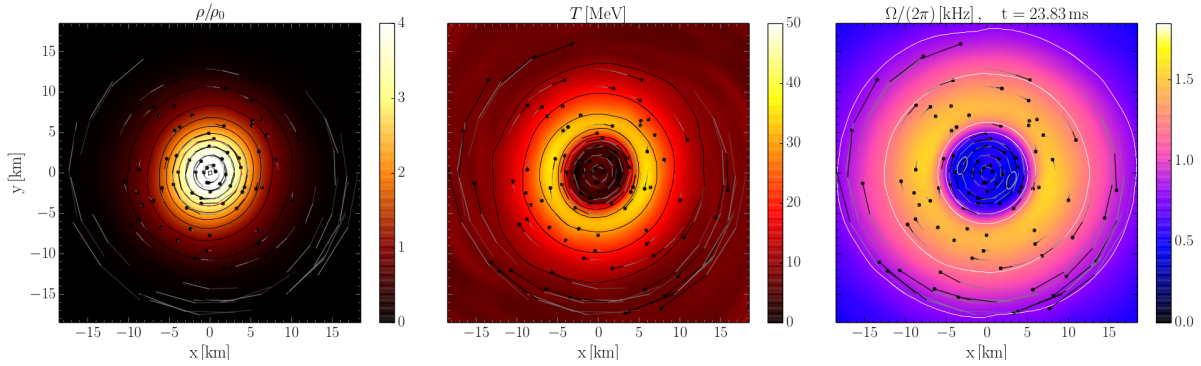

Figure A2. Same as in Figs. 3 and 4 but at a post-merger time of $t = 23.83$ ms.

References

[1] Wex N 2017 *Presentation at the DPG-Spring Meeting in Bremen, Gemany*
[2] Lyne A G, Burgay M, Kramer M, Possenti A, Manchester R N, Camilo F, McLaughlin M A, Lorimer D R, D'Amico N, Joshi B C, Reynolds J and Freire P C C 2004 *Science* **303** 1153–1157 (*Preprint* arXiv:astro-ph/0401086)
[3] Kramer M and Wex N 2009 *Class. Quantum Grav.* **26** 073001
[4] The LIGO Scientific Collaboration and the Virgo Collaboration 2016 *Phys. Rev. Lett.* **116** 061102 (*Preprint* 1602.03837)
[5] Abbott B P, Abbott R, Abbott T D, Abernathy M R, Acernese F, Ackley K, Adams C, Adams T, Addesso P, Adhikari R X and et al 2016 *Astrophys. J. Lett.* **818** L22 (*Preprint* 1602.03846)
[6] Takami K, Rezzolla L and Baiotti L 2014 *Phys. Rev. Lett.* **113** 091104 (*Preprint* 1403.5672)
[7] Takami K, Rezzolla L and Baiotti L 2015 *Phys. Rev. D* **91** 064001 (*Preprint* 1412.3240)
[8] Rezzolla L and Takami K 2016 *Phys. Rev. D* **93** 124051 (*Preprint* 1604.00246)
[9] Antoniadis J, Freire P C C, Wex N, Tauris T M, Lynch R S, van Kerkwijk M H, Kramer M, Bassa C, Dhillon V S, Driebe T, Hessels J W T, Kaspi V M, Kondratiev V I, Langer N, Marsh T R, McLaughlin M A, Pennucci T T, Ransom S M, Stairs I H, van Leeuwen J, Verbiest J P W and Whelan D G 2013 *Science* **340** 448 (*Preprint* 1304.6875)
[10] Rezzolla L and Zanotti O 2013 *Relativistic Hydrodynamics* (Oxford, UK: Oxford University Press) ISBN 9780198528906
[11] Misner C W, Thorne K S and Wheeler J A 1973 *Gravitation* (San Francisco: W. H. Freeman)
[12] Everitt C W F, Debra D B, Parkinson B W, Turneaure J P, Conklin J W, Heifetz M I, Keiser G M, Silbergleit A S, Holmes T, Kolodziejczak J, Al-Meshari M, Mester J C, Muhlfelder B, Solomonik V G, Stahl K, Worden Jr P W, Bencze W, Buchman S, Clarke B, Al-Jadaan A, Al-Jibreen H, Li J, Lipa J A, Lockhart J M, Al-Suwaidan B, Taber M and Wang S 2011 *Physical Review Letters* **106** 221101 (*Preprint* 1105.3456)
[13] Shibata M and Nakamura T 1995 *Phys. Rev. D* **52** 5428–5444
[14] Baumgarte T W and Shapiro S L 1999 *Phys. Rev. D* **59** 024007 (*Preprint* gr-qc/9810065)
[15] The Einstein Toolkit Consortium: einsteintoolkit.org
[16] Radice D, Rezzolla L and Galeazzi F 2014 *Class. Quantum Grav.* **31** 075012 (*Preprint* 1312.5004)
[17] Read J S, Lackey B D, Owen B J and Friedman J L 2009 *Phys. Rev. D* **79** 124032 (*Preprint* 0812.2163)
[18] Alford M, Braby M, Paris M and Reddy S 2005 *Astrophys. J.* **629** 969–978 (*Preprint* nucl-th/0411016)
[19] Hanauske M 2004 *Properties of Compact Stars within QCD-motivated Models* Ph.D. thesis J.W. Goethe-University Frankfurt, Germany
[20] Lattimer J M and Swesty F D 1991 *Nucl. Phys. A* **535** 331–376
[21] Mewes V, Galeazzi F, Font J A, Montero P J and Stergioulas N 2016 *Mon. Not. R. Astron. Soc.* **461** 2480–2489 (*Preprint* 1605.02629)
[22] Bovard L, Radice D and Rezzolla L 2016 *in preparation*
[23] Hanauske M, Takami K, Bovard L, Rezzolla L, Font J A, Galeazzi F and Stöcker H 2016 *arXiv preprint arXiv:1611.07152*
[24] Bleicher M *et al.* 1999 *J. Phys.* **G25** 1859–1896 (*Preprint* hep-ph/9909407)
[25] Bass S A *et al.* 1998 *Prog. Part. Nucl. Phys.* **41** 255–369 [Prog. Part. Nucl. Phys.41,225(1998)] (*Preprint* nucl-th/9803035)
[26] Mukherjee A, Steinheimer J and Schramm S 2016 (*Preprint* 1611.10144)
[27] Steinheimer J, Schramm S and Stocker H 2011 *Phys. Rev.* **C84** 045208 (*Preprint* 1108.2596)
[28] Detar C E and Kunihiro T 1989 *Phys. Rev.* **D39** 2805
[29] Hatsuda T and Prakash M 1989 *Phys. Lett.* **B224** 11–15
[30] Fukushima K 2004 *Phys. Lett.* **B591** 277–284 (*Preprint* hep-ph/0310121)
[31] Ratti C, Thaler M A and Weise W 2006 *Phys. Rev.* **D73** 014019 (*Preprint* hep-ph/0506234)
[32] Taub A H 1948 *Phys. Rev.* **74** 328–334
[33] Steinheimer J and Randrup J 2012 *Phys. Rev. Lett.* **109** 212301 (*Preprint* 1209.2462)